



BNL-99897-2013-IR

***Irradiation Experiment Conceptual Design
Parameters for NBSR Fuel Conversion***

**N. Brown, J-S. Baek, A. Hanson, A. Cuadra,
L-Y. Cheng, D. Diamond**

March 2013

Nuclear Science & Technology Department

Brookhaven National Laboratory

**U.S. Department of Energy
National Institute of Science & Technology**

Notice: This manuscript has been authored by employees of Brookhaven Science Associates, LLC under Contract No. DE-AC02-98CH10886 with the U.S. Department of Energy. The publisher by accepting the manuscript for publication acknowledges that the United States Government retains a non-exclusive, paid-up, irrevocable, world-wide license to publish or reproduce the published form of this manuscript, or allow others to do so, for United States Government purposes.

DISCLAIMER

This report was prepared as an account of work sponsored by an agency of the United States Government. Neither the United States Government nor any agency thereof, nor any of their employees, nor any of their contractors, subcontractors, or their employees, makes any warranty, express or implied, or assumes any legal liability or responsibility for the accuracy, completeness, or any third party's use or the results of such use of any information, apparatus, product, or process disclosed, or represents that its use would not infringe privately owned rights. Reference herein to any specific commercial product, process, or service by trade name, trademark, manufacturer, or otherwise, does not necessarily constitute or imply its endorsement, recommendation, or favoring by the United States Government or any agency thereof or its contractors or subcontractors. The views and opinions of authors expressed herein do not necessarily state or reflect those of the United States Government or any agency thereof.

Irradiation Experiment Conceptual Design Parameters for NBSR Fuel Conversion

Manuscript Completed:

March 29, 2013

Prepared by:

N. R. Brown, J. S. Baek, A. L. Hanson, A. Cuadra, L-Y. Cheng, and D. J. Diamond

**Nuclear Science & Technology Department
Brookhaven National Laboratory
Upton, NY 11973**

Prepared for:

**National Institute of Standards and Technology
National Nuclear Security Administration**

Abstract

It has been proposed to convert the National Institute of Standards and Technology (NIST) research reactor, known as the NBSR, from high-enriched uranium (HEU) fuel to low-enriched uranium (LEU) fuel. The motivation to convert the NBSR to LEU fuel is to reduce the risk of proliferation of special nuclear material. This report is a compilation of relevant information from recent studies related to the proposed conversion using a metal alloy of LEU with 10 w/o molybdenum. The objective is to inform the design of the mini-plate and full-size plate irradiation experiments that are being planned. This report provides relevant dimensions of the fuel elements, and the following parameters at steady state: average and maximum fission rate density and fission density, fuel temperature distribution for the plate with maximum local temperature, and two-dimensional heat flux profiles of fuel plates with high power densities. The latter profiles are given for plates in both the inner and outer core zones and for cores with both fresh and depleted shim arms (reactivity control devices). In addition, a summary of the methodology to obtain these results is presented.

Table of Contents

Abstract	iii
Table of Contents	v
List of Figures	vii
List of Tables	vii
1. Introduction.....	1
2. Geometry of the Fuel Plates, Fuel Elements, and Reactor Core	2
3. Limiting LEU Power Distribution	7
4. Limiting LEU Local Burn-Up and Fission Density.....	21
5. Limiting Fuel Temperatures.....	25
6. Summary	29
7. References.....	30

List of Figures

Figure 1 NBSR Vessel Internals and Reactor Core [1]	3
Figure 2 NBSR Fuel Element	4
Figure 3 Cross Sectional View of Fuel Element (Dimensions in Inches)	5
Figure 4 NBSR Fuel Management Scheme	6
Figure 5 Planar View of the NBSR MCNPX Model	7
Figure 6 NBSR Fuel Element Geometry in the MCNPX Model	9
Figure 7 Heat Flux Distribution, Element 8-7W, Plate 1	11
Figure 8 Heat Flux Distribution, Element 8-7W, Plate 17	12
Figure 9 Heat Flux Distribution, Element 8-3E, Plate 1	13
Figure 10 Heat Flux Distribution, Element 8-3E, Plate 17	14
Figure 11 Heat Flux Distribution, Element 8-7E, Plate 1	15
Figure 12 Heat Flux Distribution, Element 8-7E, Plate 17	16
Figure 13 Heat Flux Distribution, Element 7-2E, Plate 1	17
Figure 14 Heat Flux Distribution, Element 7-2E, Plate 17	18
Figure 15 Heat Flux Distribution, Element 8-1E, Plate 1	19
Figure 16 Heat Flux Distribution, Element 8-1E, Plate 17	20
Figure 17 LEU Cumulative Fission Density at EOC	22
Figure 18 LEU Average Axial Fission Density Distribution at Cycle 8 EOC	23
Figure 19 LEU Plate-Wise Fission Density at EOC	23
Figure 20 LEU Axial Fission Density Distribution Comparison at Cycle 8 EOC	25
Figure 21 Hydraulic Flow Channel (shown horizontally)	26
Figure 22 Heat Transfer Modeling Simplifications in a Flow Channel	27
Figure 23 Modeling of Power Distribution in the RELAP5 Input Model	28
Figure 24 Axial LEU Fuel Meat Centerline Temperature Distribution (Limiting Core Condition)	29

List of Tables

Table 1 NBSR Fuel Element Data	4
Table 2 Fraction of Fissions in the LEU NBSR	24
Table 3 Axial Fission Density Distribution at Cycle 8 EOC	25
Table 4 Values of the Requested Metrics	29

1. Introduction

This report is a compilation of results from studies of the conversion of the National Institute of Standards and Technology (NIST) research reactor, known as the NBSR, to low-enriched uranium (LEU) fuel. The objective of this document is to convey the information requested by the plate irradiation experiment design team at Idaho National Laboratory.

Brookhaven National Laboratory (BNL) has an extensive history of collaboration with NIST regarding the NBSR. BNL performed safety analysis in support of the NBSR license renewal application [1]. More recently, BNL has performed the design work and safety analysis for the LEU conversion of the NBSR. Some relevant results of these studies have been recently documented [2-7].

The following information was requested for the NBSR LEU fuel plate irradiation experiment for the most disadvantageous steady state LEU core condition [8]:

1. Nominal geometry and configuration of the fuel plates and fuel assemblies
 - a. Fuel meat thickness
 - b. Cladding thickness
 - c. Absorber thickness
 - d. Fuel assembly configuration
 - e. Fuel management scheme
2. Peak local irradiation condition at maximum licensed power
 - a. Fission density (fission/cm³)
 - b. Fission rate density (fission/cm³-s)
 - c. Heat flux distribution
 - d. Fuel meat and plate surface temperatures

This report is comprised of the following sections:

1. Introduction
2. Geometry of the Fuel Plates, Fuel Elements, and Reactor Core
3. Limiting LEU Power Distribution
4. Limiting LEU Local Burn-Up and Fission Density
5. Limiting Fuel Temperatures

The contents of Section 2 are sourced from References [1-3]. This section presents the requested information regarding the nominal LEU fuel plate and fuel element geometry. The contents of Section 3 are sourced from References [2-5]. Section 3 describes the model geometry, nodalization, fission rate density, and heat flux distribution. The heat flux distribution and fission rate density, as presented within this report, are equivalent. The contents of Section 4 are sourced from References [5-6]. Section 4 describes the average and maximum fission density as

calculated utilizing local burn-up effect studies. Section 5 is primarily sourced from Reference [3] and Reference [7]. Section 5 presents the thermal hydraulic nodalization and the relevant steady state fuel meat temperature distribution for the LEU NBSR core.

2. Geometry of the Fuel Plates, Fuel Elements, and Reactor Core

The NBSR is a high burn-up, 20 MWt reactor. The moderation and cooling is provided by D₂O, which flows upward through the core from two concentric plena just below the lower grid plate. The NBSR is designed with several unique features that enable low-energy and thermal neutrons to stream through eight radial beam tubes and two cold neutron sources. These features include an unfuelled “gap” in the axial center of the fuel elements, which contains only moderator and structural materials. This gap, which acts to minimize contamination of the streaming low-energy neutrons, is co-located with the beam tubes at the core axial mid-plane. The mid-plane gap is very significant in terms of the NBSR peak local irradiation condition. The axial thermal flux always peaks in the mid-plane gap. Because the axial location of the thermal flux peak is fixed, the fuel that is directly adjacent to the gap experiences both the highest fission rate density and the highest cumulative fission density in the NBSR core.

Another unique feature of the NBSR is the cadmium shim arms (control elements), which traverse the upper-half of the core in a semaphore fashion. During much of a reactor cycle, the shim arms act to suppress the flux in the upper half of the NBSR core. This flux “compression” shifts the peak local irradiation condition to the fuel in the lower half-element that is nearest to the mid-plane gap. A three-dimensional cut-away view of the NBSR vessel internals and reactor core is shown in Figure 1. The mid-plane gap (legend entry 5) and the shim arms (legend entry 2) are both visible in Figure 1. Due to the combined impact of the mid-plane gap and the shim arms, the local cumulative fission density in the NBSR fuel approaches 100% burn-up of fissile nuclides, primarily ²³⁵U and ²³⁹Pu.

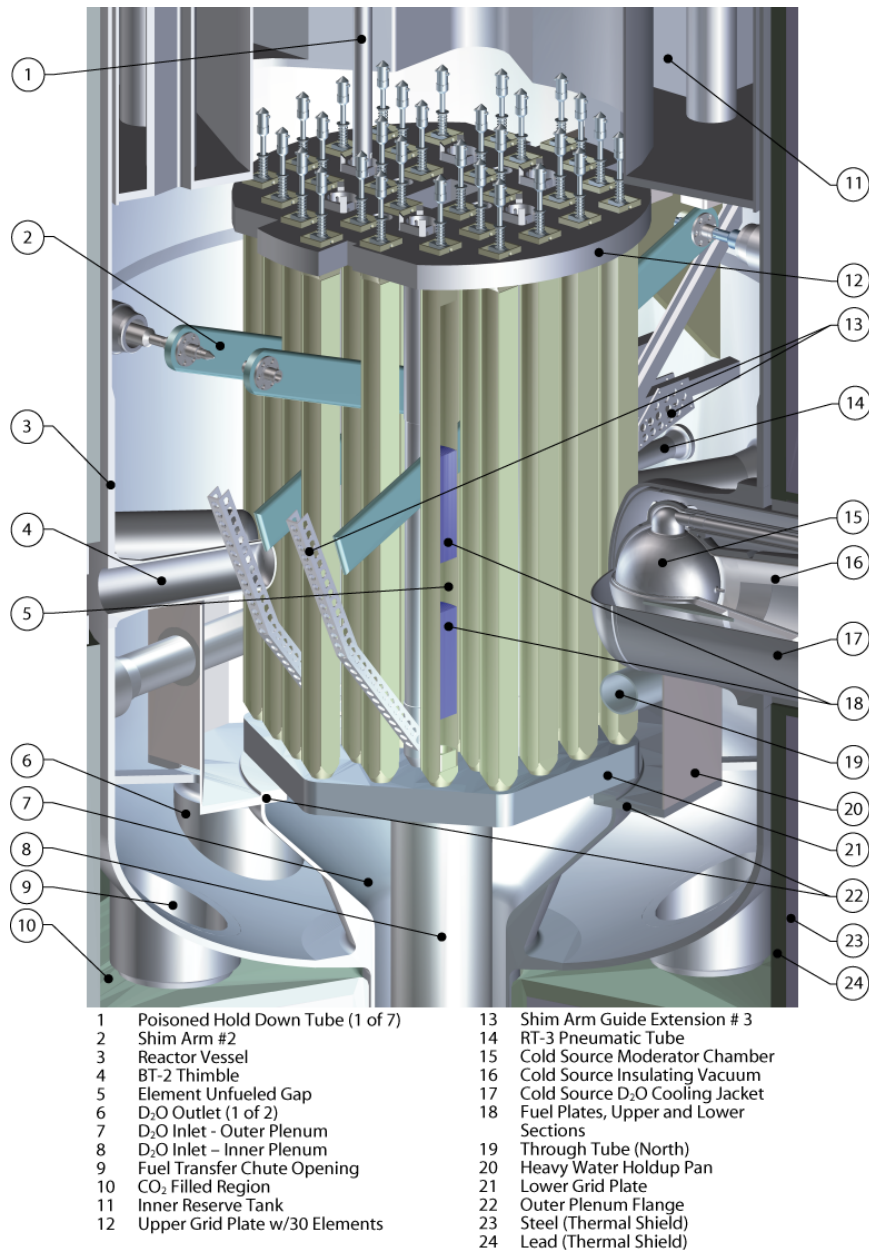


Figure 1 NBSR Vessel Internals and Reactor Core [1]

Presently, the NBSR is fueled with high-enriched uranium (HEU) with a nominal ^{235}U enrichment of 93% [1]. The fuel is U_3O_8 in an aluminum powder dispersion that is clad in aluminum alloy (Alloy 6061). Each fuel element is constructed of 17 plates in each upper and lower half (34 plates per fuel element) and is constructed in the Materials Test Reactor (MTR) curved plate geometry. Each plate is 33.02 cm (13 in) long with 27.94 cm (11 in) of fuel and the fuel width is 6.03 cm (2.373 in). The thickness of fuel meat in each plate is 0.0508 cm (0.020 in) for HEU fuel, with a volume of 148 cm^3 (9.05 in^3) of fuel per half-element. There is a 17.78 cm (7 in) gap between the upper and lower fueled regions of the core. In the gap region, the aluminum plates extend one-half inch below and above the fuel so the physical gap is 15.24 cm

(6 in). Each HEU fuel element has a mass of 350 ± 3.4 g of ^{235}U . The aluminum cladding is 0.0381 cm (0.015 in) thick on each side. Figure 2 shows the lower and upper fuel plates and the physical gap in a fuel element.

The fuel meat for the LEU conversion of the NBSR is proposed as U10Mo (10 wt% Mo alloyed with U) metal foils with the same aluminum alloy cladding used in the HEU fuel [2]. The geometrical dimensions of fuel plates in a fuel element are the same for HEU and LEU fuels except for the fuel meat and cladding thickness. Data for the nominal U10Mo fuel design are given in Table 1. The thickness of the LEU fuel foils is 0.0215 cm (0.0085 in) with a total volume of 62.64 cm^3 (3.8 in^3) per half-element. The engineering specification on fuel foil thickness is 0.0085 in. The rolling tolerance of the fuel foils is expected to be ± 0.001 in, so the fuel thickness is specified as 0.0085 ± 0.001 in. The ^{235}U content of each LEU fuel element is 383 ± 4 g, where the uncertainty is only due to the uncertainty in the molybdenum content of the LEU fuel. The 10% weight specification for molybdenum has an uncertainty of $\pm 1\%$. There is also an uncertainty in ^{235}U content due to enrichment uncertainty. The thickness of the aluminum cladding for the LEU fuel is 0.053 cm (0.0208 in) on each side. There is a 0.00254 cm (0.001 in) layer of zirconium between the cladding and the fuel to improve fuel behavior under irradiation and this is also taken into account in the modeling.

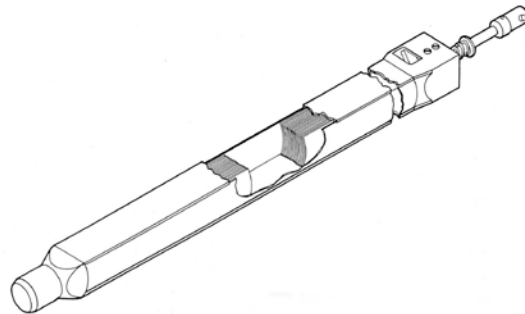


Figure 2 NBSR Fuel Element

Table 1 NBSR Fuel Element Data

Parameter	HEU	LEU
^{235}U grams	350	383
^{238}U grams	26	1556
O grams	68	0
Al grams	625	0
Mo grams	0	215
Total grams	1069	2154
Fuel density (g/cm^3)	3.61	17.2
Fuel meat thickness (cm)	0.0508	0.0215
Fuel volume, half-element (cm^3)	148	62.64

Figure 3 shows a cross sectional view of a fuel element. There are a total of 30 fuel elements in the NBSR core. Six fuel elements are located in the inner core (cooled by flow from the inner plenum) and twenty-four elements in the outer core (cooled by flow from the outer plenum). Figure 4 shows the labeling of fuel element positions. The thimble identifiers are bracketed (< >) and the regulating rod is identified as <RR>. In each position fuel elements are identified with two numbers and one letter. The letters are either E or W for the east or west side of the core noting that a fuel element always stays in the east side or in the west side of the core. The fuel management scheme of the NBSR dictates that 16 fuel elements stay in the core for eight cycles and 14 fuel elements stay in the core for seven cycles. The first number denotes how many cycles the element will be in the core (either eight or seven) and the second number denotes the cycle in which the fuel element resides. Therefore, at the beginning of a cycle, the 8-1 and 7-1 fuel elements are unirradiated fuel elements, whereas 8-8 and 7-7 are in their final cycles and will be removed after the cycle is over. After a cycle is finished the 8-8 and 7-7 fuel elements are removed and the 8-7 elements are moved into the 8-8 positions, the 7-6 elements are moved into the 7-7 positions, etc. The process proceeds until unirradiated fuel is placed in the 8-1 and 7-1 positions. The reactivity of the NBSR is controlled with four cadmium shim arms that are rotated through the core in a semaphore fashion.

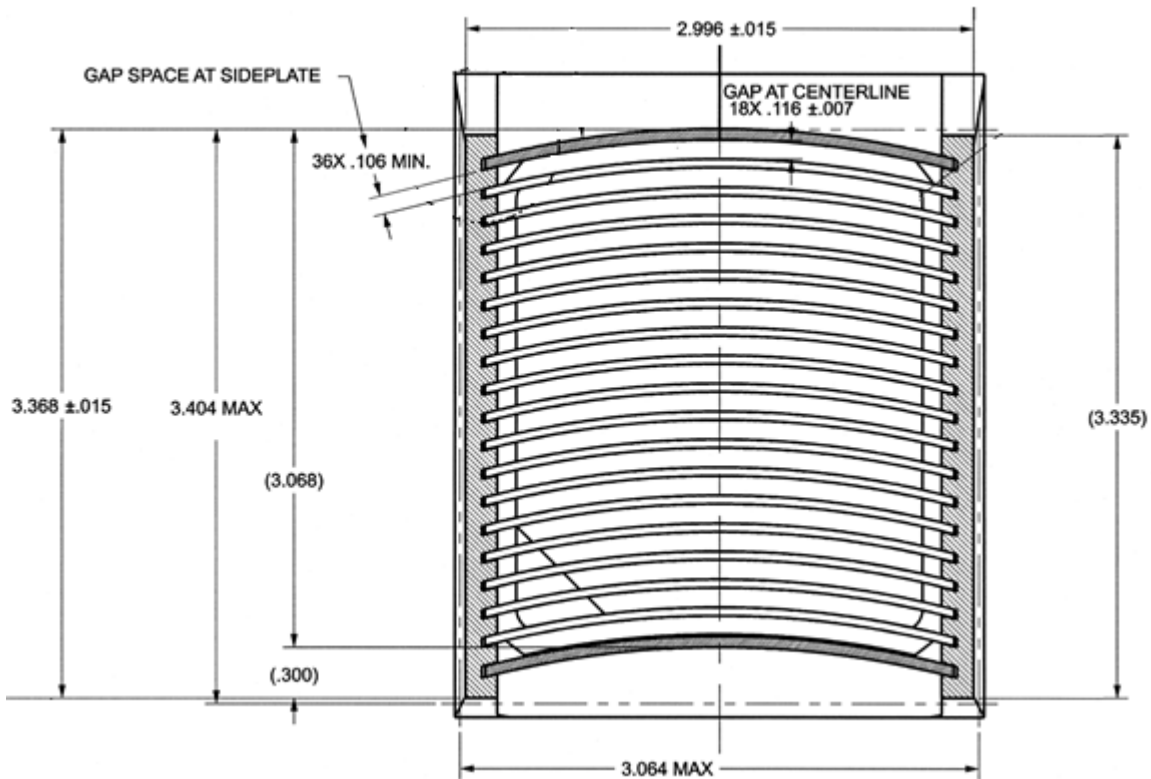


Figure 3 Cross Sectional View of Fuel Element (Dimensions in Inches)

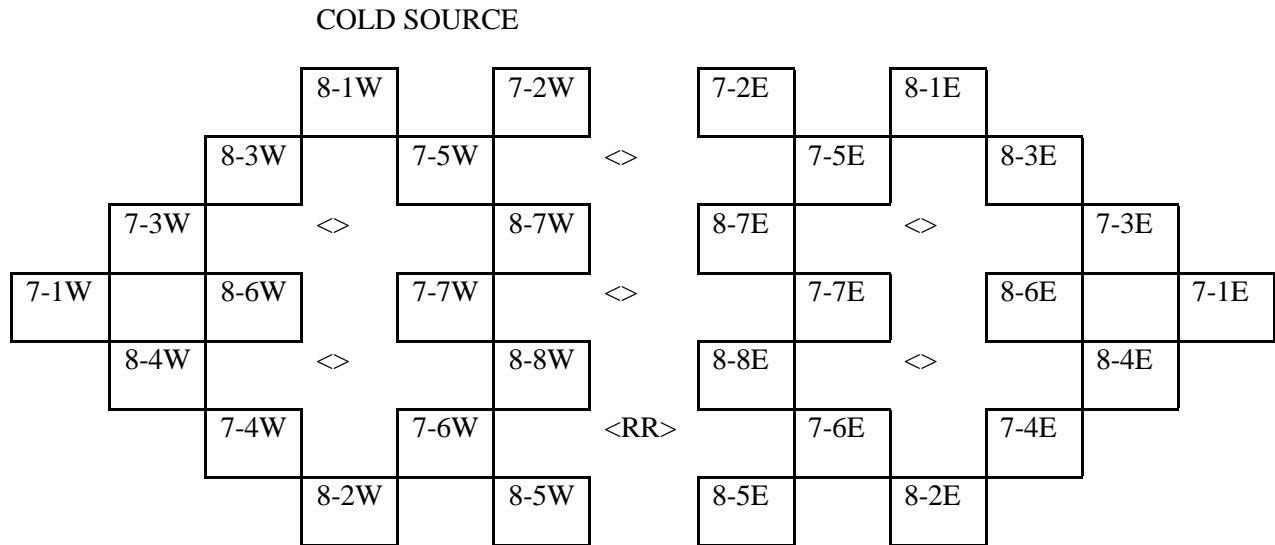


Figure 4 NBSR Fuel Management Scheme

For the conversion of the reactor to LEU fuel, an improved full-core model of the NBSR has been developed (the “present” model) for the neutronic and burn-up analysis [2]. The model utilizes MCNPX [9] to accomplish a detailed burn-up analysis where each half-element has a unique fuel inventory (material composition) that is moved throughout the core for either seven or eight 38.5-day fuel cycles. The NBSR model has been subjected to a variety of validation studies and is an evolution of the model utilized in the NBSR Safety Analysis Report [1]. It has also been utilized to design two cold neutron sources, and to compute the prompt neutron lifetime [2]. A planar view of the NBSR model is shown in Figure 5. Some of the specific improvements made to the burn-up analysis in the present full-core model include [2]:

- reduction in unaccounted mass from ~1.2% per cycle per fuel element to ~0.13% per cycle per fuel element
- increase of the number of isotopes considered from a maximum of 63 to a maximum of 210
- increase of the number of fuel inventories from 30 to 60 eliminating forced symmetry radially, in the half fuel elements’ material compositions
- inclusion of the 10.5-day decay time at the end of each cycle
- analysis of additional burn-up state points
- utilization of the ENDF-B/VII.0 cross section libraries
- realistic positioning of the shim arms (control elements) within each burn-up state point

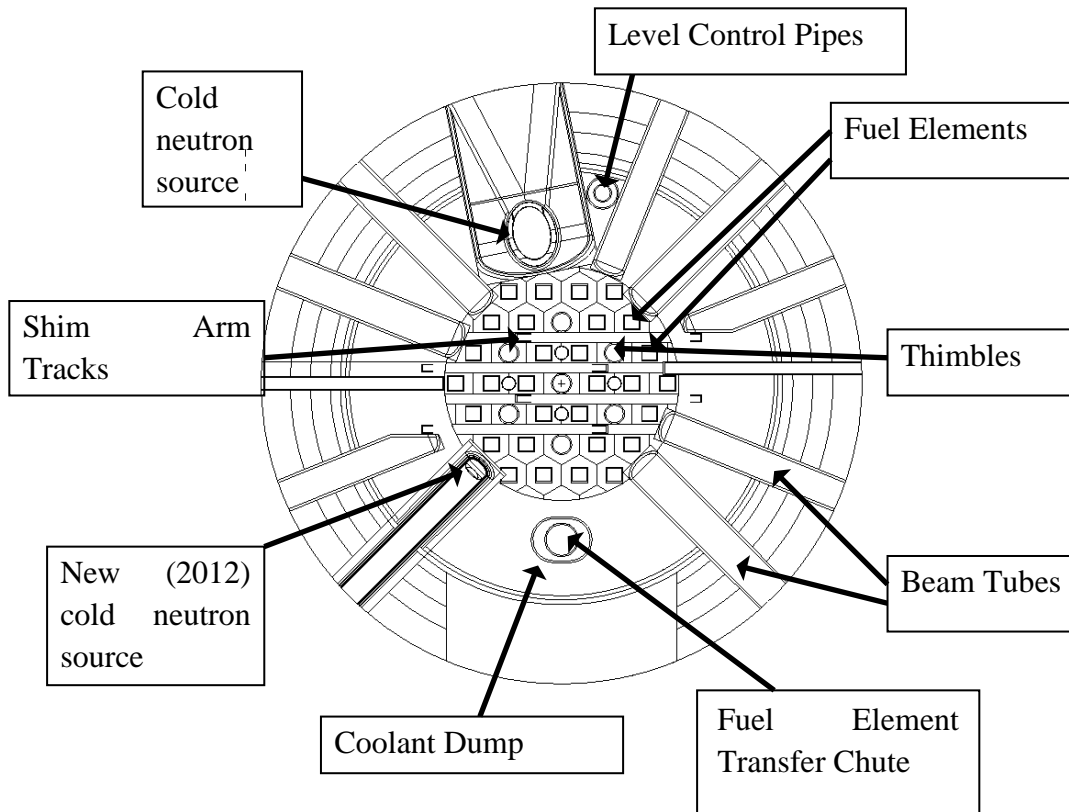


Figure 5 Planar View of the NBSR MCNPX Model

3. Limiting LEU Power Distribution

The purpose of this section is to inform the design and planning of future irradiation experiments by documenting the calculated fission rate density and heat flux distribution in the LEU NBSR. For evaluation of the fission distribution in the NBSR core, a large number of nodes for the fuel plates were used in the MCNPX analysis [3]. Figure 6 shows an elevation view with the axial discretization of the fuel element geometry in the MCNPX model. The plates are modeled without curvature for simplification. The choice of mesh size for the MCNPX calculations is based on the observation that heat conduction in a fuel plate will result in a lateral heat flux profile (i.e. across the width of a fuel plate) that is flatter than the profile of the energy deposition due to fission [10]. The heat conduction problem was analyzed both analytically [10] and numerically [11]. The results indicate the average surface energy flux (sum of energy deposition divided by the surface area of a mesh cell) for a 4 cm² mesh conservatively captures the maximum wall heat flux determined by solving the heat conduction problem for a fuel plate. Using this information as guidance for the evaluation of power distribution in the core, the MCNPX calculations employed mesh cells (nodes) with a width of about 2 cm and a height of about 2 cm. There are three cells in the lateral direction and 14 cells in the axial direction per fuel plate. The total number of cells used for the MCNPX analysis is calculated as below.

$$N_{TOT-C} = (\text{Number of cells in lateral direction}) \cdot (\text{Number of cells in axial direction}) \\ \cdot (\text{Number of plates per fuel element}) \cdot (\text{Number of fuel elements})$$

$$N_{TOT-C} = 3 \times 14 \times (2 \times 17) \times 30 = 42,840$$

The number of fissions in each cell has been calculated for HEU and LEU fuels at startup (SU), the limiting core condition in terms of the local heat flux and fission rate density, and end-of-cycle (EOC), the limiting core condition in terms of the fission density. It is assumed that all fission energy is deposited directly in the NBSR fuel and within the cell that contains the fission. This assumption is conservative because in reality a small fraction of the fission energy will be deposited directly in the cladding, coolant, moderator, and reactor structural material. Detailed descriptions of the evaluation of power distribution and kinetic parameters by using the MCNPX computer code are presented in [2].

The average fission rate density in the NBSR is calculated based on the core power, the number of nodes in the core, and the volume of each node. The dimensions of each node are 1.9957 cm \times 2.04 cm \times 0.0215 cm. In the proposed LEU U10Mo fuel the average fission rate density is,

$$\begin{aligned} \text{Average fission rate density} \left[\frac{\text{fission}}{\text{cm}^3 - \text{s}} \right] &= (\text{core thermal power}) \times \frac{1}{(\text{fuel volume})} \\ &= \frac{20 \times 10^6 \text{W}}{200 \times 10^6 \text{eV} \times 1.602 \times 10^{-19} \frac{\text{J}}{\text{eV}}} \\ &\times \frac{1}{42840 \times 1.9957 \text{ cm} \times 2.04 \text{ cm} \times 0.0215 \text{ cm}} = 1.657 \times 10^{14} \frac{\text{fission}}{\text{cm}^3 - \text{s}} \end{aligned}$$

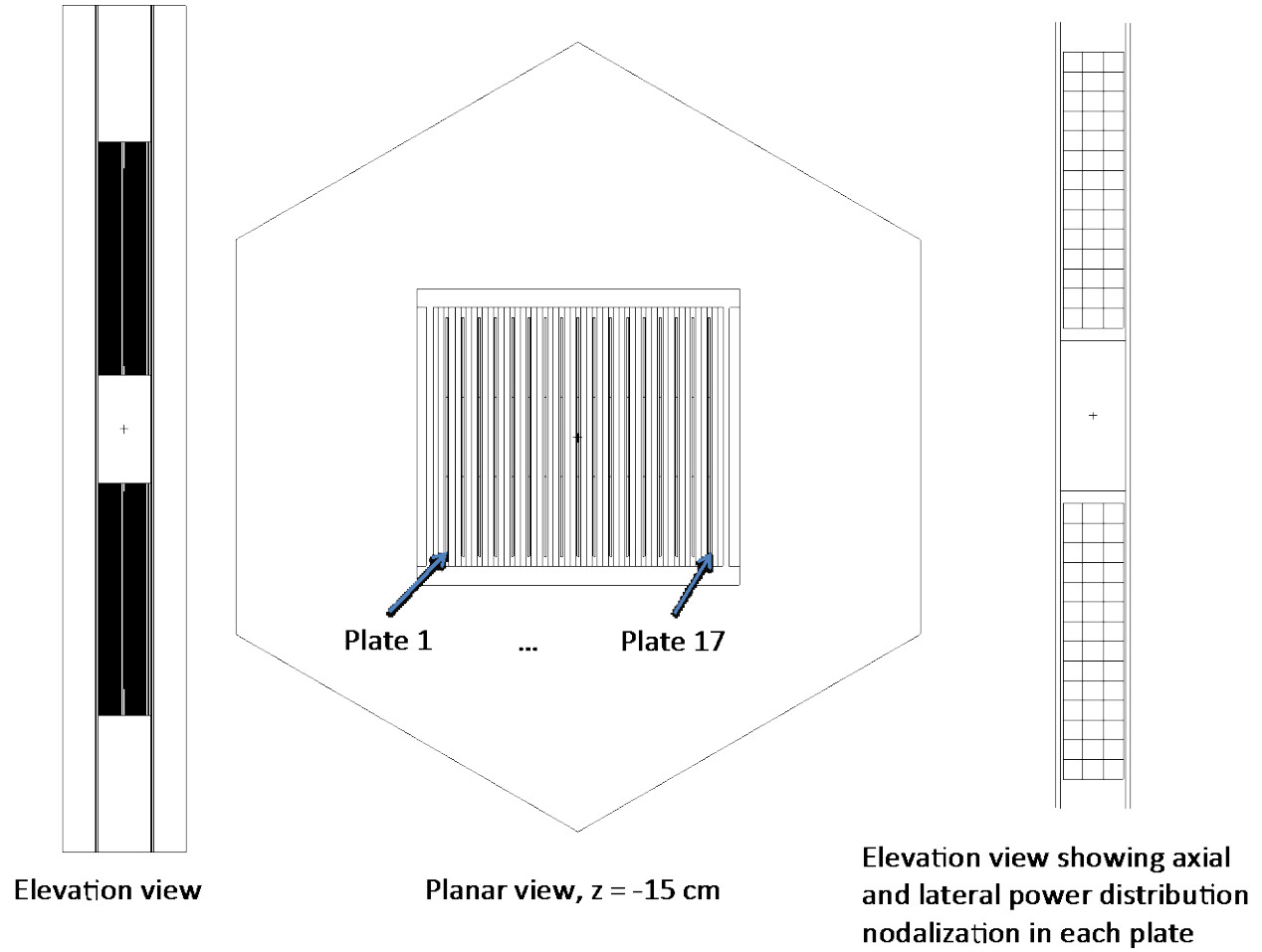


Figure 6 NBSR Fuel Element Geometry in the MCNPX Model

The maximum fission rate density is calculated utilizing the average fission rate density and the node peaking factor. The node peaking factor is the ratio of the peak number of fissions-per-node to the average number of fissions per node, as calculated utilizing the MCNPX model. For the proposed LEU fuel the maximum fission rate density is,

$$\begin{aligned} \text{Maximum fission rate density} \left[\frac{\text{fission}}{\text{cm}^3 - \text{s}} \right] &= (\text{average fission rate density}) \times (\text{node peaking factor}) \\ &= 1.657 \times 10^{14} \frac{\text{fission}}{\text{cm}^3 - \text{s}} \times 2.431 = 4.029 \times 10^{14} \frac{\text{fission}}{\text{cm}^3 - \text{s}} \end{aligned}$$

The limiting core heat flux distribution occurs at SU with fresh shim arms. The core power is more evenly distributed when the shim arms are withdrawn from the core or in a depleted state, because the flux compression in the upper-half of the NBSR core (due to the shim arms) is reduced. This reduces the magnitude of the hot spots and increases the minimum critical heat flux ratio (CHFR). The plate-wise heat flux distributions are plotted in Figure 7 - Figure 10 for the elements with hot spots (maximum number of fissions-per-node) and in Figure 11 - Figure 14 for the elements with hot stripes (maximum number of fissions per vertical stripe). Plots are included for both Plate 1 and Plate 17; however, due to the orientation of the fuel elements within the core, the hot spots and hot stripes always occur in plate 17. In addition to the limiting cases, the heat flux distributions are also provided for a fresh element, 8-1E, in Figure 15 and Figure 16.

The axial dimension of the fuel element is relative to the axial center of the mid-plane gap ($z = 0.0$ cm) and the lateral dimension is relative to the lateral center of the fuel plate ($y=0.0$ cm). The node maximum heat flux of 1394 kW/m^2 , corresponding to the maximum fission rate density and a peaking factor of 2.431, occurs on plate 17 of element 8-3E. Element 8-3E is a relatively fresh element, having experienced only two 38.5 day cycles of irradiation. Heat flux distributions are shown for both the inner and outer flow plenum locations. Additionally, the heat flux distributions are shown with fresh shim arms and with shim arms that have been irradiated for twenty-five cycles. The heat flux distribution results for irradiated shim arms are derived from the results of a recent study [9]. To convert a local heat flux to a fission rate density,

$$\text{Fission rate density} \left[\frac{\text{fission}}{\text{cm}^3 - \text{s}} \right] = q'' \left(\frac{\text{kW}}{\text{m}^2} \right) \times 2.890 \times 10^{11} \frac{\text{fission}}{\text{cm}^3 - \text{s}} \left(\frac{\text{m}^2}{\text{kW}} \right)$$

		<i>Element 8-7W</i>			<i>Plate 1</i>			<i>Inner plenum</i>		
		Lateral position (cm)						Lateral position (cm)		
		2.04	0.00	-2.04				2.04	0.00	-2.04
Axial position (cm)	U p p e r	Fresh shim arms			Heat flux (kW/m ²)	Depleted shim arms				
36.8		381	384	419	1400	421	425	465		
34.8		401	395	425	1200	453	431	493		
32.8		468	415	481	1000	483	434	497		
30.8		522	486	517	800	517	483	577		
28.8		552	497	582	600	565	525	587		
26.9		600	546	612	400	619	556	617		
24.9		636	609	661	200	656	602	672		
22.9		701	638	704		700	643	698		
20.9		751	702	725		765	683	762		
18.9		800	712	778		792	718	790		
16.9		877	789	854		874	781	851		
14.9		954	852	928		951	862	917		
12.9		1009	961	1020		1067	959	1029		
10.9		1228	1141	1196		1250	1155	1205		
0.0										
-10.9		1364	1292	1328		1319	1253	1291		
-12.9		1201	1057	1186		1160	1063	1153		
-14.9		1093	1015	1081		1066	965	1044		
-16.9		1046	934	1027		1012	907	977		
-18.9		991	910	985		983	884	943		
-20.9		961	882	942		960	849	933		
-22.9		930	863	937		907	819	894		
-24.9		930	830	903		902	798	884		
-26.9		908	802	855		876	780	851		
-28.8		875	791	892		861	767	860		
-30.8		892	764	825		850	758	830		
-32.8		871	785	834		850	755	837		
-34.8		892	814	858		844	787	855		
-36.8		952	905	932		908	852	901		
	L o w e r									

Figure 7 Heat Flux Distribution, Element 8-7W, Plate 1

		<i>Element 8-3E</i>			<i>Plate 1</i>			<i>Outer plenum</i>		
		Lateral position (cm)						Lateral position (cm)		
		2.04 0.00 -2.04						2.04 0.00 -2.04		
Axial position (cm)		Fresh shim arms			Heat flux (kW/m ²)	Depleted shim arms				
36.8	U p p e r	305	364	459	1400	416	464	545		
34.8		265	332	427	1200	365	392	505		
32.8		261	325	432	1000	363	387	504		
30.8		309	344	465	800	363	387	490		
28.8		358	368	473	600	432	417	505		
26.9		411	410	479	400	436	437	526		
24.9		467	452	551	200	505	468	564		
22.9		539	489	577		533	503	583		
20.9		583	521	589		599	546	625		
18.9		660	585	631		657	587	657		
16.9	708	618	664		702	625	681			
14.9	785	667	721		780	668	751			
12.9	849	745	768		841	751	807			
10.9	1040	928	947		1018	915	927			
0.0										
-10.9	L o w e r	1178	1043	1047		1158	1053	1034		
-12.9		1039	898	923		1025	892	944		
-14.9		954	845	919		961	819	893		
-16.9		921	812	858		931	796	859		
-18.9		895	782	863		910	793	859		
-20.9		937	749	830		886	769	816		
-22.9		872	747	824		864	745	822		
-24.9		872	746	800		864	743	783		
-26.9		861	740	799		820	737	789		
-28.8		862	740	841		816	705	780		
-30.8	831	737	799		784	730	781			
-32.8	850	734	803		837	733	794			
-34.8	878	778	828		833	731	823			
-36.8	922	868	927		927	839	881			

Figure 9 Heat Flux Distribution, Element 8-3E, Plate 1

		<i>Element 8-3E</i>	<i>Plate 17</i>		<i>Outer plenum</i>	<i>Hot spot (SU)</i>					
		Lateral position (cm)	2.04	0.00	-2.04	2.04	0.00	-2.04			
Axial position (cm)	U p p e r	Fresh shim arms			Heat flux (kW/m²)	Depleted shim arms					
		36.8	313	386		487	1400	423	456	538	
		34.8	306	345		425	1200	399	428	509	
		32.8	332	379		442	1000	411	423	514	
		30.8	404	409		466	800	455	434	506	
		28.8	466	421		521	600	501	469	542	
		26.9	540	459		529	400	545	502	564	
		24.9	603	521		587	200	606	529	583	
		22.9	644	561		635		654	593	626	
		20.9	710	606		653		700	611	662	
		18.9	762	656		729		767	641	718	
		16.9	820	719		750		821	709	752	
		14.9	901	766		811		909	782	827	
		12.9	987	862		903		1008	866	919	
		10.9	1144	1032		1062		1187	1099	1076	
		0.0									
		L o w e r	-10.9	1394		1194	1216		1348	1189	1199
			-12.9	1216		995	1075		1177	1003	1015
	-14.9		1115	935	952		1091	926	945		
	-16.9		1037	875	923		1039	884	897		
	-18.9		1025	830	903		1010	836	870		
-20.9	956		830	876		981	820	840			
-22.9	987		805	857		939	787	844			
-24.9	912		829	816		933	768	833			
-26.9	928		764	814		908	765	797			
-28.8	926		791	796		896	756	763			
-30.8	938		742	788		865	743	803			
-32.8	891		750	800		906	750	792			
-34.8	883	792	854		915	763	795				
-36.8	1017	919	935		990	869	909				

Figure 10 Heat Flux Distribution, Element 8-3E, Plate 17

		<i>Element 8-7E</i>			<i>Plate 1</i>			<i>Inner plenum</i>		
		Lateral position (cm)						Lateral position (cm)		
		2.04	0.00	-2.04				2.04	0.00	-2.04
Axial position (cm)	U p p e r	Fresh shim arms			Heat flux (kW/m ²)	Depleted shim arms				
36.8		387	354	330	1400	420	387	398		
34.8		403	357	347	1200	432	378	418		
32.8		428	394	406	1000	472	419	444		
30.8		485	453	486	800	499	443	492		
28.8		523	494	535	600	556	487	533		
26.9		589	534	572	400	582	540	576		
24.9		641	568	606	200	648	591	619		
22.9		661	605	667		670	628	688		
20.9		751	641	731		725	670	715		
18.9		775	713	786		775	709	784		
16.9		862	789	824		836	771	833		
14.9		909	825	914		914	834	885		
12.9		1048	905	1028		1011	934	980		
10.9		1183	1104	1176		1199	1111	1182		
0.0										
	L o w e r									
-10.9		1355	1277	1321		1332	1242	1295		
-12.9		1187	1102	1164		1149	1069	1149		
-14.9		1074	977	1075		1051	966	1055		
-16.9		1033	940	1036		1019	930	1012		
-18.9		985	899	1019		985	874	935		
-20.9		960	876	957		928	839	925		
-22.9		945	812	910		931	820	885		
-24.9		920	828	896		894	830	880		
-26.9		896	822	887		875	795	862		
-28.8		851	795	863		839	759	824		
-30.8		875	807	836		832	760	809		
-32.8		872	781	834		856	768	813		
-34.8		878	799	847		841	789	832		
-36.8		944	875	948		927	862	900		

Figure 11 Heat Flux Distribution, Element 8-7E, Plate 1

<i>Element 8-7E</i>		<i>Plate 17</i>			<i>Inner plenum</i>			<i>Hot stripe (SU)</i>			
Lateral position (cm)		2.04	0.00	-2.04				2.04	0.00	-2.04	
Axial position (cm)	U p p e r	Fresh shim arms			Heat flux (kW/m²)	Depleted shim arms					
		36.8	388	375		366	1400	427	417	423	
		34.8	426	379		418	1200	463	409	444	
		32.8	466	440		450	1000	489	441	494	
		30.8	500	465		522	800	539	461	521	
		28.8	533	521		532	600	560	511	571	
		26.9	612	548		587	400	591	557	611	
		24.9	640	612		665	200	655	597	647	
		22.9	672	621		705		694	644	703	
		20.9	728	676		734		758	667	732	
		18.9	820	734		777		802	714	790	
		16.9	877	770		840		865	768	836	
		14.9	972	861		922		937	849	910	
		12.9	1037	934		1039		1034	947	1023	
		10.9	1247	1138		1174		1213	1148	1169	
		0.0									
		L o w e r	-10.9	1345		1255	1339		1301	1229	1284
			-12.9	1186		1093	1175		1174	1061	1149
			-14.9	1125		1016	1078		1092	941	1054
			-16.9	1032		946	1013		1019	916	989
-18.9	978		896	979		971	847	943			
-20.9	955		873	960		927	844	926			
-22.9	934		837	911		936	827	915			
-24.9	958		832	913		890	812	870			
-26.9	891		794	896		880	805	850			
-28.8	916		839	854		862	787	856			
-30.8	875		799	847		874	756	825			
-32.8	888		785	857		863	754	828			
-34.8	895		832	897		873	804	860			
-36.8	947		918	918		933	864	909			

Figure 12 Heat Flux Distribution, Element 8-7E, Plate 17

		<i>Element 7-2E</i>			<i>Plate 1</i>			<i>Outer plenum</i>		
Lateral position (cm)		2.04	0.00	-2.04				2.04	0.00	-2.04
Axial position (cm)		Fresh shim arms			Heat flux (kW/m ²)	Depleted shim arms				
36.8	Upper	741	683	734	1400	781	719	789		
34.8		661	593	661	1200	698	632	701		
32.8		645	557	658	1000	676	615	693		
30.8		651	587	639	800	668	600	671		
28.8		648	594	645	600	697	616	693		
26.9		679	589	671	400	717	607	694		
24.9		688	572	671	200	738	646	716		
22.9		729	618	736		735	654	705		
20.9		795	654	713		774	672	757		
18.9		830	690	750		826	701	773		
16.9		866	693	782		872	739	803		
14.9		929	800	839		933	788	851		
12.9		1007	849	925		1020	898	950		
10.9		1204	1058	1110		1230	1070	1098		
0.0										
-10.9		Lower	1269	1116	1168		1284	1120	1134	
-12.9			1114	952	968		1098	929	983	
-14.9	1018		839	917		1020	832	902		
-16.9	931		796	844		942	794	848		
-18.9	906		740	821		888	760	809		
-20.9	851		728	778		870	710	789		
-22.9	881		694	747		846	706	748		
-24.9	856		683	766		842	678	729		
-26.9	828		677	749		798	661	728		
-28.8	786		659	716		804	646	685		
-30.8	766		626	702		760	643	678		
-32.8	775		646	688		781	628	665		
-34.8	811		672	708		783	657	672		
-36.8	883		805	778		882	767	769		

Figure 13 Heat Flux Distribution, Element 7-2E, Plate 1

		<i>Element 7-2E</i>	<i>Plate 17</i>		<i>Outer plenum</i>	<i>Hot stripe (SU)</i>					
		Lateral position (cm)	2.04	0.00	-2.04	2.04	0.00	-2.04			
Axial position (cm)	U p p e r	Fresh shim arms			Heat flux (kW/m²)	Depleted shim arms					
		36.8	781	703		779	1400	816	740	790	
		34.8	736	614		688	1200	763	668	727	
		32.8	738	615		682	1000	741	663	701	
		30.8	739	628		683	800	745	648	711	
		28.8	727	649		700	600	780	639	715	
		26.9	765	643		679	400	780	659	724	
		24.9	798	670		707	200	806	695	724	
		22.9	791	689		732		830	696	765	
		20.9	870	733		807		855	741	762	
		18.9	889	724		817		887	754	814	
		16.9	950	764		845		937	794	831	
		14.9	1021	842		881		1001	833	881	
		12.9	1074	916		955		1104	933	970	
		10.9	1311	1145		1145		1310	1127	1131	
		0.0									
		L o w e r		1363		1197	1183		1351	1136	1185
			-10.9	1181		996	1041		1160	993	984
			-12.9	1110		881	912		1058	901	911
			-14.9	1029		867	890		1024	830	890
-16.9	1005		811	870		992	821	849			
-18.9	985		783	829		946	769	787			
-20.9	947		762	807		905	754	763			
-22.9	920		752	765		903	739	739			
-24.9	901		715	740		862	714	753			
-26.9	853		708	736		858	709	724			
-28.8	866		706	740		848	694	697			
-30.8	858		675	737		853	696	713			
-32.8	849		726	736		857	694	718			
-34.8	957	809	808		930	791	790				
-36.8											

Figure 14 Heat Flux Distribution, Element 7-2E, Plate 17

		<i>Element 8-1E</i>	<i>Plate 1</i>	<i>Outer plenum</i>	<i>Fresh Element</i>			
Lateral position (cm)		2.04	0.00	-2.04	2.04 0.00 -2.04			
Axial position (cm)	Fresh shim arms			Heat flux (kW/m ²)	Depleted shim arms			
36.8	Upper	680	656	725	1400	737	687	744
34.8		613	557	663	1200	637	633	678
32.8		570	541	604	1000	644	584	657
30.8		585	543	643	800	644	575	672
28.8		609	571	625	600	643	585	666
26.9		631	584	665	400	656	595	687
24.9		628	610	655	200	663	603	675
22.9		666	593	684		701	620	691
20.9		713	627	714		698	624	725
18.9		726	627	755		725	645	756
16.9		760	644	768		760	668	748
14.9		801	676	784		815	727	790
12.9		874	768	820		874	766	855
10.9		1030	892	963		1010	925	959
0.0								
-10.9		Lower	1092	956	985		1079	961
-12.9	949		814	858		950	819	894
-14.9	881		760	827		888	747	809
-16.9	866		759	820		845	748	778
-18.9	851		701	789		831	713	790
-20.9	816		728	771		801	693	772
-22.9	822		722	750		786	679	754
-24.9	781		694	739		774	682	738
-26.9	775		670	731		758	652	725
-28.8	804		671	724		753	646	684
-30.8	744		638	700		758	648	699
-32.8	766		645	701		771	630	684
-34.8	772		660	704		777	666	689
-36.8	869		782	768		857	761	759

Figure 15 Heat Flux Distribution, Element 8-1E, Plate 1

		<i>Element 8-1E</i>			<i>Plate 17</i>			<i>Outer plenum</i>			<i>Fresh Element</i>								
		Lateral position (cm)									Lateral position (cm)								
		2.04			0.00			-2.04			2.04			0.00			-2.04		
Axial position (cm)								Heat flux (kW/m ²)											
		Fresh shim arms			Depleted shim arms				Fresh shim arms			Depleted shim arms							
36.8		701	651	752	1400	745	737	781											
34.8		632	591	669	1200	674	606	708											
32.8	U	620	566	634	1000	642	605	658											
30.8	p	587	587	656	800	644	595	676											
28.8	p	595	571	663	600	663	585	701											
26.9	e	665	594	653	400	687	593	713											
24.9	r	664	624	702	200	694	619	682											
22.9		713	633	699		710	654	722											
20.9		735	664	747		732	664	752											
18.9		759	716	769		771	678	755											
16.9		834	705	793		801	746	802											
14.9		886	762	806		886	782	830											
12.9		927	873	916		970	843	910											
10.9		1135	1011	1038		1149	1048	1063											
0.0																			
-10.9		1195	1067	1098		1191	1085	1097											
-12.9		1049	908	957		1016	904	947											
-14.9	L	975	862	882		930	820	885											
-16.9	o	896	770	837		887	751	822											
-18.9	w	856	736	804		844	758	812											
-20.9	e	851	743	824		832	733	808											
-22.9	r	834	723	797		817	682	761											
-24.9		818	696	748		790	695	739											
-26.9		775	669	761		780	668	729											
-28.8		769	649	706		771	650	711											
-30.8		763	672	721		742	633	696											
-32.8		737	649	693		771	630	664											
-34.8		798	670	703		758	662	694											
-36.8		885	765	801		874	761	773											

Figure 16 Heat Flux Distribution, Element 8-1E, Plate 17

4. Limiting LEU Local Burn-Up and Fission Density

The purpose of this section is to inform the design and planning of future irradiation experiments by documenting the calculated cumulative fission density in the LEU NBSR. The calculation of the average cumulative fission density depends on the average fission rate density and the average core residence time (7.5 cycles of 38.5 days),

$$\begin{aligned} \text{Average fission density} \left[\frac{\text{fission}}{\text{cm}^3} \right] &= (\text{average fission rate density}) \times (\text{core residence time}) \\ &= 1.657 \times 10^{14} \frac{\text{fission}}{\text{cm}^3 - \text{s}} \times 7.5 \times 38.5 \text{ day} \times \frac{86400 \text{ s}}{\text{day}} = 4.134 \times 10^{21} \frac{\text{fission}}{\text{cm}^3} \end{aligned}$$

The maximum fission density depends on the local burn-up. In the equilibrium LEU core model the fuel inventories are homogenized within each half-element. However, recent studies have investigated the distribution of burn-up within the NBSR half-element [5]. These studies have shown two effects: (1) the impact of the mid-plane gap on axial burn-up and (2) the impact of the plate-to-plate self-shielding on the plate-wise burn-up. The impact of these two effects has not been considered synergistically. The study was accomplished via a single element model without shim arms. Thus, the impact of the shim arms, which will increase the local fission density in the lower half-element and decrease the local fission density in the upper half-element, is not reflected in these results. However, these results provide a useful estimate of the “average” of the upper and lower half-element axial fission density distribution and illustrate the impact of the mid-plane gap on the local fission density due to thermal flux peaking.

Two models are utilized to study two local burn-up effects separately. One model utilizes an axial burn-up cell nodalization, and the other model utilizes a plate-wise cell nodalization. The study of axial burn-up distribution used an axial nodalization that is the same as the nodalization used to extract the power distribution, but the plate-wise and lateral nodalization is not the same. The main difference between the nodalization in the axial burn-up model and the nodalization in the power distribution full-core model, is that the axial nodes span all seventeen plates within the axial burn-up model. Additionally, each axial node also spans all three lateral nodes. Because the shim arms are not included in the models utilized for local burn-up quantification, the upper and lower half-elements are symmetric, for a total of fourteen unique axial depletion nodes. The cumulative EOC axial burn-up is shown as fission density in Figure 17 and the LEU axial fission density distribution at EOC of Cycle 8 is shown in Figure 18. In Figure 17 Node 1 represents the two depletion nodes closest to the mid-plane gap and Node 14 represents the two depletion nodes on the top and bottom of the fuel element. The colors correspond to the different nodes. Due to the large number of nodes some colors are repeated. The axial height of the fuel element is relative to the axial center of the mid-plane gap ($z = 0.0$ cm). The mid-plane gap is evident in Figure 18.

In the plate-wise burn-up case nine plates are considered, with each plate treated as a single burn-up node, accounting for symmetry within the fuel element (eight “symmetric” plates and one central plate). For example, Plate 1 is considered to be symmetric with Plate 17, Plate 2 is symmetric with Plate 16, etcetera. The cumulative plate-wise burn-up is shown as fission density in Figure 19.

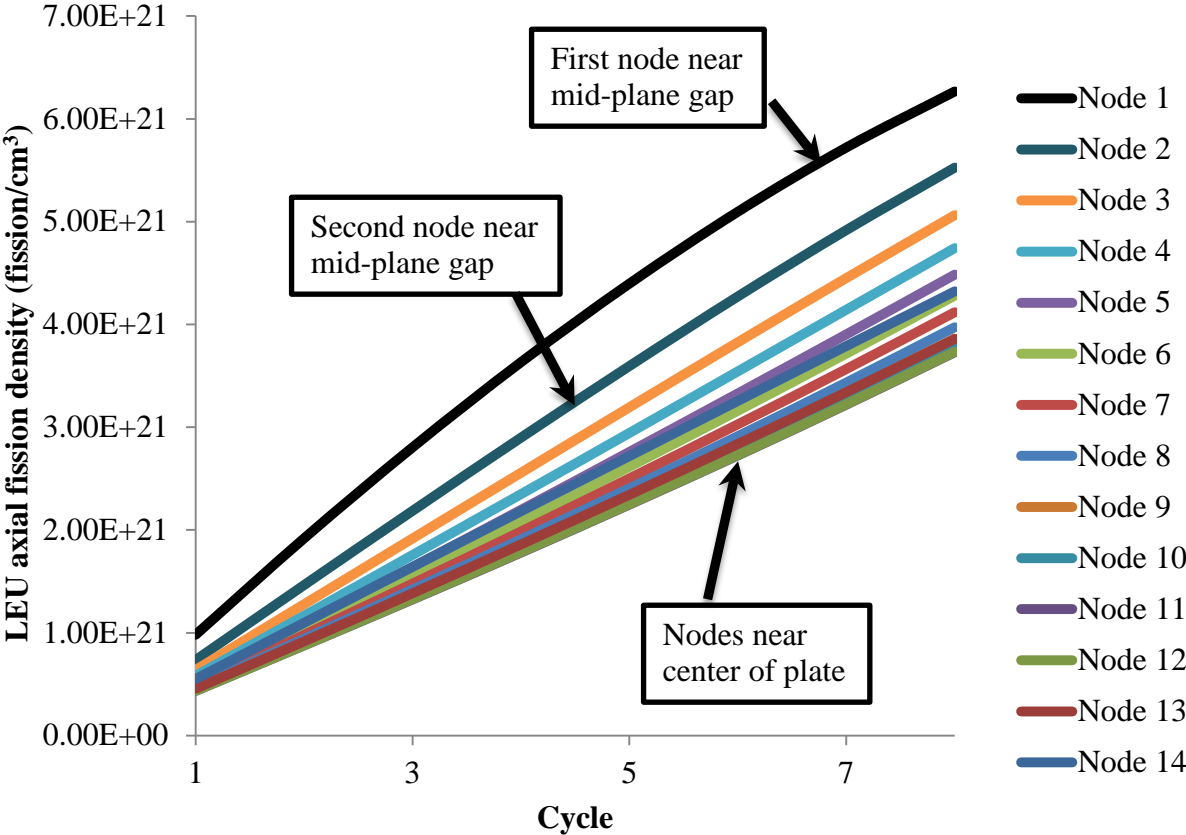


Figure 17 LEU Cumulative Fission Density at EOC

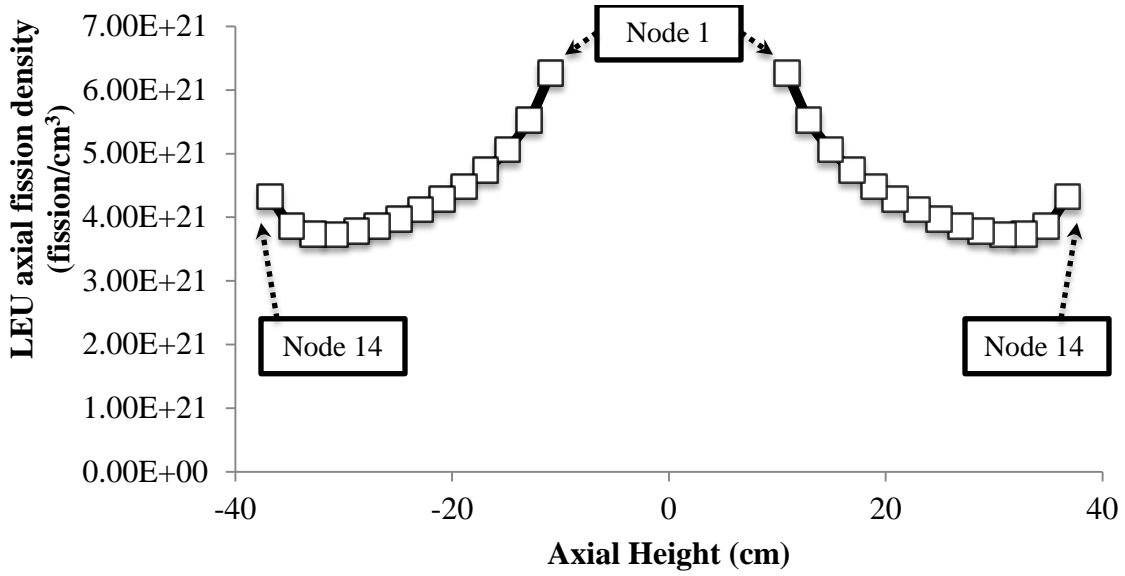


Figure 18 LEU Average Axial Fission Density Distribution at Cycle 8 EOC

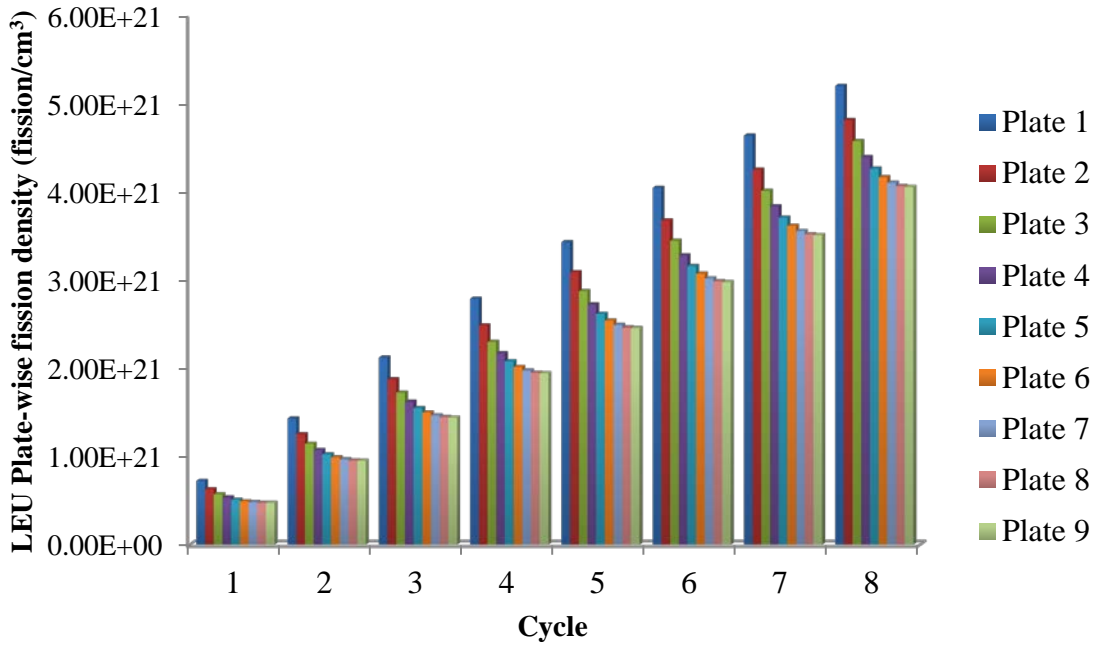


Figure 19 LEU Plate-Wise Fission Density at EOC

To approximate the maximum fission density, the maximum node burn-up at eight cycles was divided by the average node burn-up at 7.5 cycles to yield axial and plate-wise burn-up factors. The maximum fission density, which would occur at an outer fuel plate that is adjacent to the mid-plane gap, is calculated as,

$$\begin{aligned}
 \text{Maximum fission density} & \left[\frac{\text{fission}}{\text{cm}^3} \right] \\
 & \approx (\text{average fission density}) \times \frac{(\text{maximum axial burnup})}{(\text{average axial burnup})} \times \frac{(\text{maximum plate – wise burnup})}{(\text{average plate – wise burnup})} \\
 & = 4.134 \times 10^{21} \frac{\text{fission}}{\text{cm}^3} \times \frac{150.5 \text{ GWd/t}}{99.29 \text{ GWd/t}} \times \frac{124.4 \text{ GWd/t}}{98.81 \text{ GWd/t}} = 7.888 \times 10^{21} \frac{\text{fission}}{\text{cm}^3}
 \end{aligned}$$

This approximate calculation is physically realizable only if there is sufficient available fissile material to accommodate this local fission density. The initial atom density of ^{235}U is,

$$\begin{aligned}
 \text{Initial atom density of } U - 235 & \left[\frac{\text{atom}}{\text{cm}^3} \right] = \frac{(\text{mass of } U - 235)}{(\text{fuel volume})} \times \frac{(6.022 \times 10^{23} / \text{mol})}{(235.04 \text{ g/mol})} \\
 & = \frac{(383 \text{ g})}{(62.6408 \text{ cm}^3 \times 2)} \times \frac{(6.022 \times 10^{23} \text{ atom})}{(235.04 \text{ g})} = 7.833 \times 10^{21} \frac{\text{atom}}{\text{cm}^3}
 \end{aligned}$$

The average atom density of ^{239}Pu at EOL (cycle 8) is,

$$\begin{aligned}
 \text{Cycle 8 atom density of } Pu - 239 & \left[\frac{\text{atom}}{\text{cm}^3} \right] = \frac{(\text{mass of } Pu - 239)}{(\text{fuel volume})} \times \frac{(6.022 \times 10^{23} / \text{mol})}{(239.05 \text{ g/mol})} \\
 & = \frac{(7.20 \text{ g})}{(62.6408 \text{ cm}^3 \times 2)} \times \frac{(6.022 \times 10^{23} \text{ atom})}{(239.05 \text{ g})} = 0.145 \times 10^{21} \frac{\text{atom}}{\text{cm}^3}
 \end{aligned}$$

Thus, the calculated fission density is physically realizable in the LEU NBSR. To provide context, Table 2 shows the fraction of fissions that occur due to each fissile or fissionable nuclide in the LEU NBSR [2]. At SU and EOC, the two fissile nuclides ^{235}U and ^{239}Pu account for over 99% of fissions in the LEU NBSR. The local burn-up of ^{235}U will certainly approach 100% within the NBSR.

Table 2 Fraction of Fissions in the LEU NBSR

	LEU SU	LEU EOC
^{235}U	96.35	95.71
^{236}U	0.02	0.02
^{238}U	0.49	0.49
^{239}Pu	2.99	3.54
^{241}Pu	0.16	0.24

By utilizing the plate-wise burn-up factors the axial fission density distribution is approximated for several plates in Figure 20. Figure 20 highlights the fact that the majority of the fuel plates result in similar cumulative burn-up, with the exception of the outer plates. The fission densities values plotted in Figure 20 are shown in Table 3.

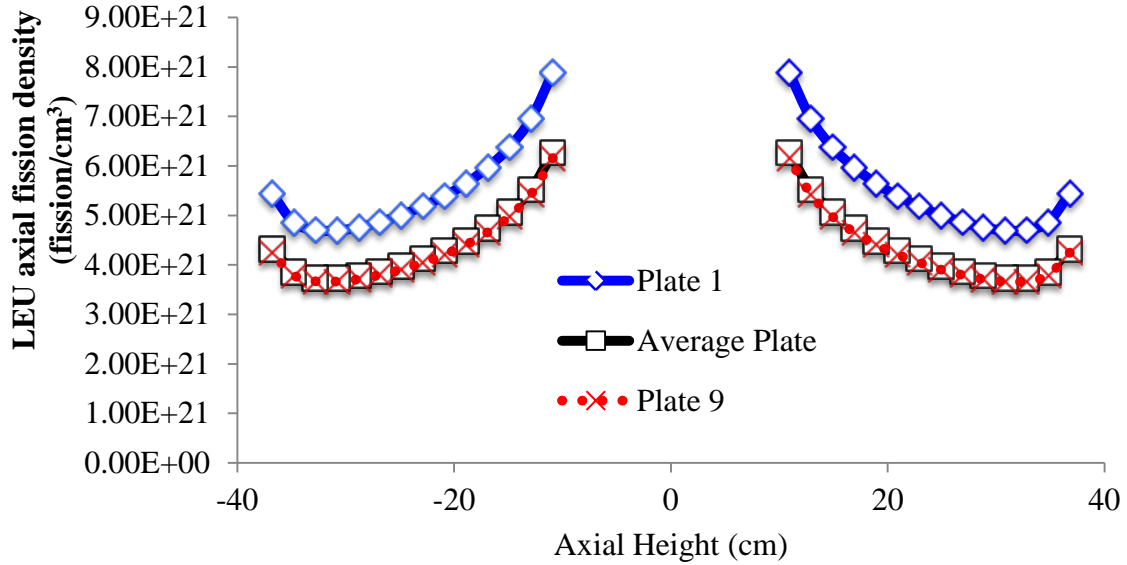


Figure 20 LEU Axial Fission Density Distribution Comparison at Cycle 8 EOC

Table 3 Axial Fission Density Distribution at Cycle 8 EOC

Fission density (fission/cm ³)			
Axial Height (\pm cm)	Plate 1	Average Plate	Plate 9
10.9	7.889E+21	6.266E+21	6.158E+21
12.9	6.956E+21	5.525E+21	5.430E+21
14.9	6.374E+21	5.063E+21	4.975E+21
16.9	5.971E+21	4.742E+21	4.660E+21
18.9	5.646E+21	4.484E+21	4.407E+21
20.9	5.389E+21	4.280E+21	4.206E+21
22.9	5.185E+21	4.119E+21	4.047E+21
24.9	5.001E+21	3.973E+21	3.904E+21
26.9	4.863E+21	3.862E+21	3.795E+21
28.8	4.754E+21	3.776E+21	3.711E+21
30.8	4.695E+21	3.729E+21	3.664E+21
32.8	4.700E+21	3.733E+21	3.669E+21
34.8	4.858E+21	3.858E+21	3.792E+21
36.8	5.441E+21	4.322E+21	4.247E+21

5. Limiting Fuel Temperatures

The thermal-hydraulic safety analysis for the NBSR has been documented in Reference 7. The tool utilized for the safety analysis is RELAP5. As described in Reference 3, the power distributions in the RELAP5 model are derived from the full-core power distributions calculated using MCNPX. The channels with hot spots and hot stripes are modeled using a conservative

methodology to simplify the power distributions calculated with MCNPX. Nuclear hot channel factors (for example, local power peaking) are modeled but engineering hot channel factors (for example, uncertainties in fuel meat thickness) are not explicitly considered in this analysis. A summary of some relevant assumptions is included here, but full discussion may be found elsewhere [3].

In the RELAP5 model, five flow channels are used to model the six inner plenum fuel elements and eight flow channels are used to represent the twenty-four outer plenum fuel elements. It is assumed in the NBSR model that the core channel flow paths are connected in parallel and the power to each channel is determined based on the fission distribution calculated by MCNPX. Each core channel has heat structures representing the fuel plates in the lower and upper core regions. A core channel may represent multiple fuel plates lumped together as an effective plate with an effective flow channel representing the flow through the plated and un-plated regions. The RELAP5 analysis only accounts for one-dimensional heat transfer from the fuel to the coolant and no axial or lateral heat conduction in the fuel plate is modeled. A hydraulic flow channel is shown in Figure 21.

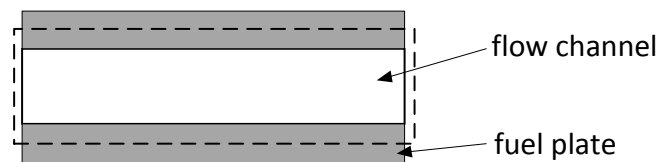


Figure 21 Hydraulic Flow Channel (shown horizontally)

The heat generated in a fuel plate is transferred to the two adjacent flow channels. In the analysis it is assumed that the power generated in the hottest plate is transferred into one common flow channel as shown in the lower diagram in Figure 22. This is conservative for two reasons. Firstly, the hottest plate, by definition, is next to a plate that is not as hot (plate A in Figure 22) and secondly, it is observed from the power distribution analysis that the hottest plate is always the outer-most plate in a fuel element. The latter means that one side of the hottest plate faces a channel that has an unfueled aluminum plate on the other side (plate B in Figure 22) and hence, has cooler water on that side. The heat flux into this cooler outside channel q''_B is more than the average heat flux from the hottest plate and the heat flux into the hot channel q''_A will actually be less than the average heat flux (q'') from that plate.

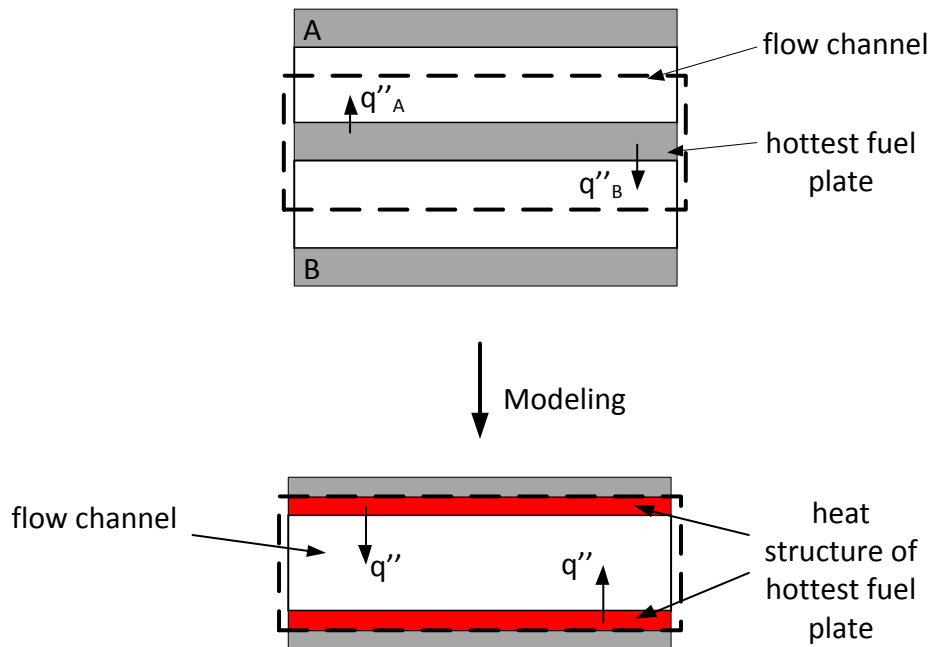


Figure 22 Heat Transfer Modeling Simplifications in a Flow Channel

The power distribution in the NBSR core is modeled using heat structures for flow channels. A FORTRAN program has been developed to read the very detailed fission information in each cell, as calculated by MCNPX. The program examines the hottest cells where the highest power is produced in the inner and outer core plenum.

The power distributions are examined along the axial cells that include the hottest cell. This is called a “fuel stripe” and represents one-third of a fuel plate. This is illustrated in Figure 23. The model is conservatively simplified by assuming that the power distribution in the hottest axial stripe is the same in the remaining two lateral stripes. This methodology is illustrated in Figure 23.

The steady state axial fuel meat centerline temperature distribution is shown in Figure 24 for the most limiting LEU core condition. Even though the methodology for obtaining the power distribution in RELAP5 is conservative, the predicted fuel meat temperatures are less than 390 K for all nodes.

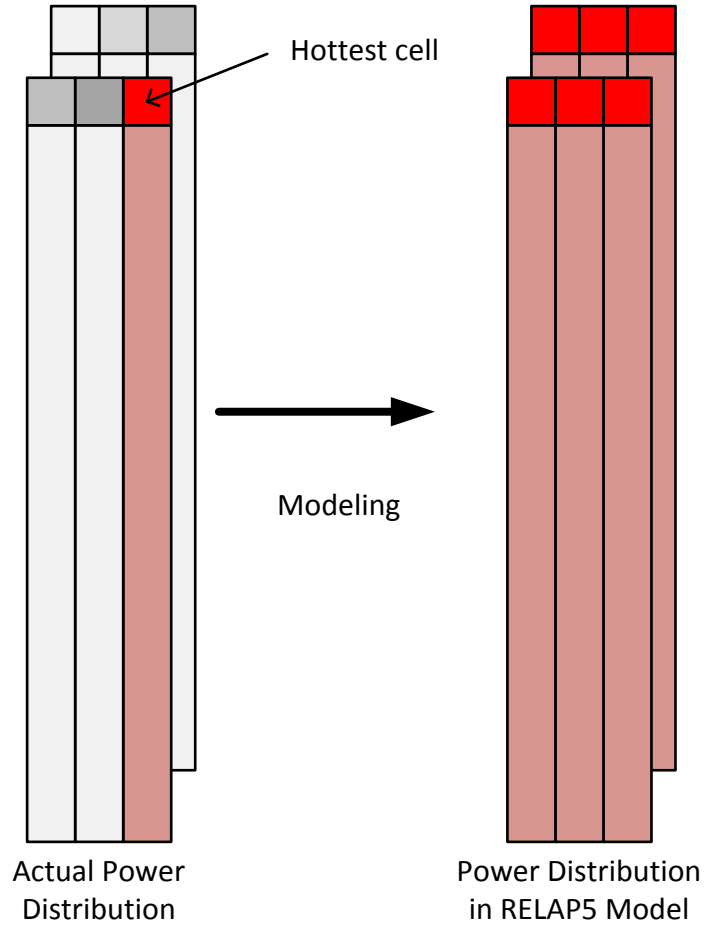


Figure 23 Modeling of Power Distribution in the RELAP5 Input Model

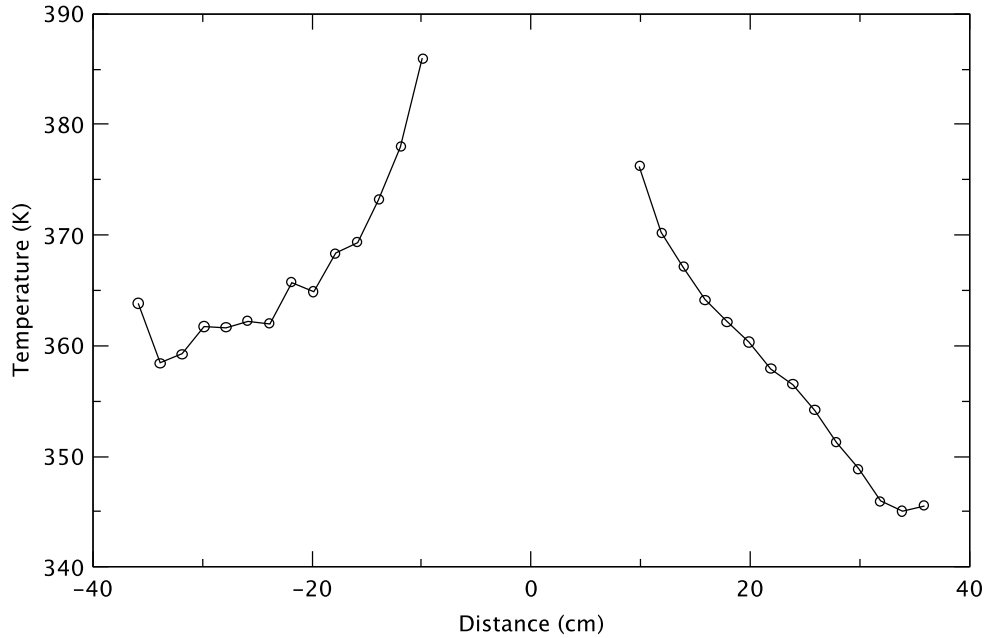


Figure 24 Axial LEU Fuel Meat Centerline Temperature Distribution (Limiting Core Condition)

6. Summary

This report presents a compilation of requested information relevant to the design of irradiation experiments for the LEU NBSR fuel. This report is intended to provide only the significant highlights of the LEU NBSR core design and safety analysis. An effort has been made to present best-estimate results for the most limiting LEU core conditions. The channels with hot spots and hot stripes were modeled with a methodology for simplifying the core power distributions that produces conservative results. Additional detail regarding the methods utilized in the calculations is provided in the relevant references, although the context and presentation differs from this document. A summary of some of the requested metrics is presented in Table 3.

Table 4 Values of the Requested Metrics

Parameter	Value
Average fission rate density (10^{14} fission/cm ³ -s)	1.657
Peak fission rate density (10^{14} fission/cm ³ -s)	4.029
Average heat flux (kW/m ²)	573
Peak heat flux (kW/m ²)	1394
Average fission density (10^{21} fission/cm ³)	4.134
Peak fission density (10^{21} fission/cm ³)	7.888
Fuel meat temperature (K)	< 390

7. References

- [1] NIST, "Safety Analysis Report (SAR) for License Renewal for the National Institute of Standards and Technology Reactor - NBSR; NBSR-14, Rev. 4," U.S. Department of Commerce, NISTIR 7102, National Institute of Standards and Technology, 2010. Note that this is a modified version of the original NBSR-14 issued in 2004.
- [2] A. L. Hanson and D. J. Diamond, "Calculation of Design Parameters for an Equilibrium LEU Core in the NBSR," BNL Technical Report, Brookhaven National Laboratory, September 29, 2011.
- [3] J-S. Baek, "Power Distribution in NBSR Core for RELAP5 Safety Analysis," BNL Technical Report, Brookhaven National Laboratory, May 25, 2012.
- [4] A. L. Hanson, N. R. Brown, and D. J. Diamond, "Effect of Shim Arm Depletion in the NBSR," BNL Technical Report (BNL-99764-2013-IR), Brookhaven National Laboratory, February 21, 2013.
- [5] N. R. Brown, A. L. Hanson, and D. J. Diamond, "Local Burn-Up Effects in the NBSR Fuel Element," BNL Technical Report (BNL-99145-2013-IR), Brookhaven National Laboratory, January 23, 2013.
- [6] A. L. Hanson, "The Maximum Burnup in an NBSR Fuel Element," BNL Memorandum, Brookhaven National Laboratory, February 9, 2012.
- [7] J-S. Baek, A. Cuadra, A. L. Hanson, L-Y. Cheng, N. R. Brown, and D.J. Diamond, "Accident Analysis for the NIST Research Reactor Before and After Fuel Conversion," BNL Technical Report (BNL-98524-2012-IR), Brookhaven National Laboratory, September 27, 2012.
- [8] E. H. Wilson, "Irradiation Conceptual Design Parameters," Electronic mail communication, Argonne National Laboratory, February 4, 2013.
- [9] D.B. Pelowitz, "MCNPX Users Manual Version 2.7.0," LA-CP-11-00438, Los Alamos National Laboratory, 2011.
- [10] J. M. Rowe, "Choice of Mesh Size for Hot Strips," NIST Memorandum, National Institute of Standards and Technology, May 15, 2008.
- [11] L-Y. Cheng, "Heat Conduction in a NBSR Fuel Plate – Effect on Wall Heat Flux," BNL Memorandum, Brookhaven National Laboratory, April 6, 2010.